



UNIVERSITÉ  
LAVAL

# Broadband silicon photonic polarimeter using subwavelength grating metamaterial waveguides

Zhongjin Lin and Wei Shi

SPIE Photonics West Conference 2020

© 2020 SPIE. Personal use of this material is permitted. Permission from SPIE must be obtained for all other uses, in any current or future media, including reprinting/republishing this material for advertising or promotional purposes, creating new collective works, for resale or redistribution to servers or lists, or reuse of any copyrighted component of this work in other works.

# PROCEEDINGS OF SPIE

[SPIDigitalLibrary.org/conference-proceedings-of-spie](https://spiedigitallibrary.org/conference-proceedings-of-spie)

## Broadband silicon photonic polarimeter using subwavelength grating metamaterial waveguides

Lin, Zhongjin, Shi, Wei

Zhongjin Lin, Wei Shi, "Broadband silicon photonic polarimeter using subwavelength grating metamaterial waveguides," Proc. SPIE 11284, Smart Photonic and Optoelectronic Integrated Circuits XXII, 112841K (26 February 2020); doi: 10.1117/12.2548519

**SPIE.**

Event: SPIE OPTO, 2020, San Francisco, California, United States

# Broadband silicon photonic polarimeter using subwavelength grating metamaterial waveguides

Zhongjin Lin<sup>a</sup> and Wei Shi<sup>a</sup>

<sup>a</sup>Department of Electrical and Computer Engineering, Centre for Optics, Photonics and Laser (COPL), Université Laval, Québec, QC G1V 0A6, Canada

## ABSTRACT

In this work, we address a chip-scale polarimeter in which the measurement frame remains optimal over a wavelength range of 200 nm in the presence of Gaussian and Poisson shot noise. The optimization includes equalized variances of each Stokes parameter, and minimal equally weighted variance. The proposed device contains only four photodetectors, which is the minimum number required for full-Stokes reconstruction. It includes broadband asymmetric power splitters and phase shifters. Notably, the broadband phase shifters are designed based on the subwavelength grating waveguides.

**Keywords:** polarimetry, chip-level, silicon, optimization problem, photonic integrated circuit

## 1. INTRODUCTION

The accuracy of a polarimeter is determined by its architecture as well as the noise of the photodetector (PD).<sup>1</sup> Due to the fact that significantly decreasing PD noise is costly, improving polarimeter performance through its architecture is typically preferred. Recently, we reported several chip-level polarimeters that perform optimally in the presence of Gaussian and Poisson shot noise.<sup>2-4</sup> Our previously designed polarimeter that has six PDs is able to maintain its optimal performance over a wide range of wavelengths.<sup>3</sup> However, according to our previous analyses, the division-of-amplitude polarimeters (DOAP) with four PDs have the minimum equally weighted variances (EWV) in the presence of the same Gaussian noise.<sup>2</sup> Due to the absence of a broadband non-90 degree phase shifter (PS), we were unable to create a broadband optimal polarimeter with four PDs.<sup>2</sup>

Several broadband PSs have been reported, including tapered PS, asymmetric PS, and asymmetric subwavelength grating (SWG) PS.<sup>5,6</sup> Recently, the SWG PS has been demonstrated to be the best choice for substantially expanding the operational wavelength range of an integrated PS.<sup>6</sup> In our previous work, we used the conventional waveguides to generate phase differences. However, the phase difference was inversely proportional to the wavelength. Thus, our previous four-PD polarimeter could not remain optimal over a broad wavelength range.<sup>2</sup> Here, we propose a broadband four-PD polarimeter based on SWG waveguides. The SWG PSs used in our device are more complicated than the conventional ones because of the need to compensate for the phase differences generated by the asymmetric power splitter. Therefore, we will first systematically study the optical properties of the SWG waveguide and SWG PSs. Then, we will present the various PSs that can be formed. Finally, we will design a broadband polarimeter using these PSs.

## 2. WAVELENGTH-INDEPENDENT PHASE SHIFTER

In this paper, all structures are designed for the standard 220-nm-thick silicon-on-insulator (SOI) material platform. Three-dimensional finite-difference time-domain (FDTD) simulations were performed to study the optical properties of our devices. In the simulations, the dispersion of Si and SiO<sub>2</sub> was taken into account. The mesh used for our 3D-FDTD simulations was 10 nm in all directions.

---

Further author information: (Send correspondence to Wei Shi)

Zhongjin Lin: E-mail: zhongjin.lin.1@ulaval.ca, Telephone: +1 418 656 2131 ext. 416188

Wei Shi: E-mail: wei.shi@gel.ulaval.ca, Telephone: +1 418 656 2131 ext. 3315

## 2.1 SWG waveguide

Figure 1(a) presents the schematic of the SWG waveguide. The width of the interconnection waveguide is  $W_{in} = 500$  nm. We set period  $\Lambda$  of the grating at 200 nm. A duty cycle of 50% is applied, *i.e.*  $a = b = 100$  nm. Firstly, we set the length of the input and output tapers at  $L_T = 3$   $\mu\text{m}$ . We then fixed the number of periods at 50 and changed the width  $W$  of the SWG waveguide. Figures 1(b)-(e) show the field distributions at 1550 nm in the SWG waveguides when  $W = 1.3$   $\mu\text{m}$ , 1.5  $\mu\text{m}$ , 1.6  $\mu\text{m}$ , and 1.8  $\mu\text{m}$ , respectively. In all these figures, the light propagates from left to right. The higher order modes are not excited until  $W$  is larger than 1.6  $\mu\text{m}$ . In other words, the phenomenon of multimode interference is not a concern when  $W$  is smaller than 1.6  $\mu\text{m}$ .

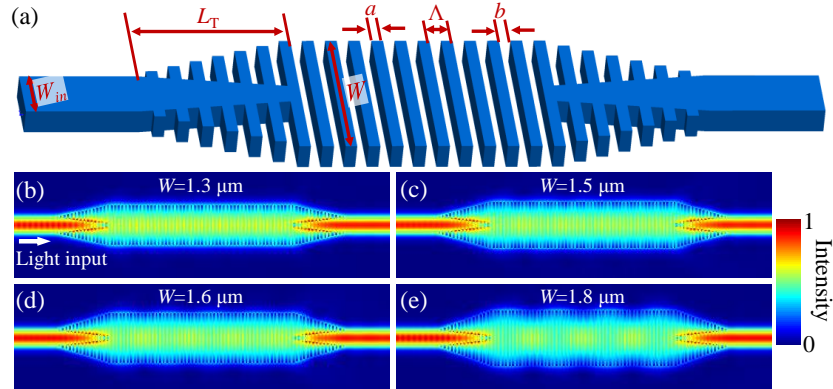


Figure 1. (a) The schematic of the SWG waveguide. (b)-(e) are the electrical field distributions of the SWG waveguides for  $W = 1.3$   $\mu\text{m}$ , 1.5  $\mu\text{m}$ , 1.6  $\mu\text{m}$ , and 1.8  $\mu\text{m}$ , respectively. For all SWG waveguides,  $L_T = 3$   $\mu\text{m}$ .

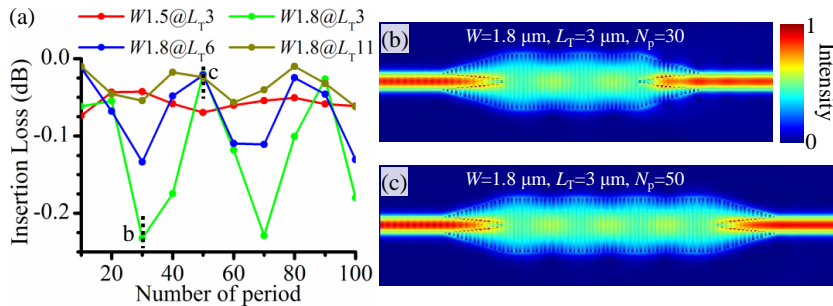


Figure 2. (a) Insertion losses of SWG waveguides as a function of the number of period when  $W = 1.5$   $\mu\text{m}$  and  $L_T = 3$   $\mu\text{m}$  ( $W1.5@L_T3$ ),  $W = 1.8$   $\mu\text{m}$  and  $L_T = 3$   $\mu\text{m}$  ( $W1.8@L_T3$ ),  $W = 1.8$   $\mu\text{m}$  and  $L_T = 6$   $\mu\text{m}$  ( $W1.8@L_T6$ ), respectively. (b) and (c) are the electrical field distributions of  $W1.8@L_T3$  when the number of period is equal to 30 and 50, respectively.

To design a PS in which the phase shift can be arbitrarily selected, multimode interference in the waveguide needs to be avoided because it induces significant variations in the insertion loss associated the length of the waveguide. As shown in Fig 2(a), when  $W = 1.5$   $\mu\text{m}$  and  $L_T = 3$   $\mu\text{m}$ , the insertion loss is insensitive with the number of periods. However, there is a significant change in the insertion loss associated with the number of periods ( $N_p$ ) when the  $L_T$  is short and the  $W$  is wide. Figures 2(b) and 2(c) present the field distributions of the SWG waveguide with a width of 1.8  $\mu\text{m}$  and a taper length of 3  $\mu\text{m}$ , when the insertion loss achieves maximum and minimum values, respectively. The green, blue, and dark gold lines in Fig 2(a) illustrate that an increasing  $L_T$  can weaken the amount of the multimode interference.

## 2.2 Asymmetric SWG PS

Figure 3 is a schematic of the asymmetric SWG PS. It consists of two SWG waveguides with different widths ( $W_U$  and  $W_L$ ). Here, we denote the accumulated phase difference between two SWG waveguides as  $\Phi$ . González-Andrade et al. used a design where  $W_U = 1.8$   $\mu\text{m}$ ,  $W_L = 1.6$   $\mu\text{m}$ , and  $L_T = 3$   $\mu\text{m}$  to achieve a broadband 90° phase shift between two waveguides.<sup>6</sup> As discussed above, the SWG waveguide when  $W_U = 1.8$   $\mu\text{m}$  and

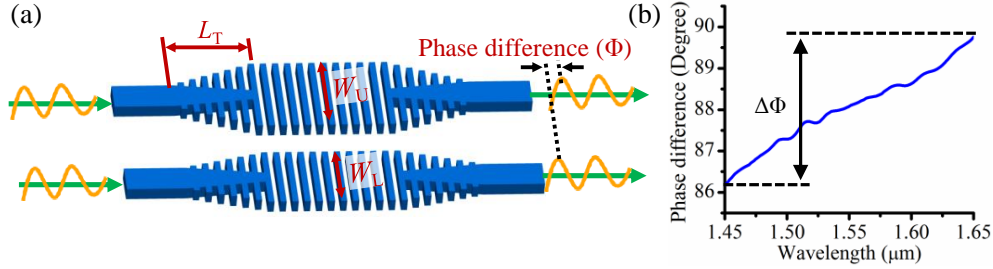


Figure 3. (a) A schematic of the SWG PS. (b) The phase difference as a function of the wavelength when  $W_U = 1.8 \mu\text{m}$ ,  $W_L = 1.6 \mu\text{m}$ , and  $L_T = 3 \mu\text{m}$ .

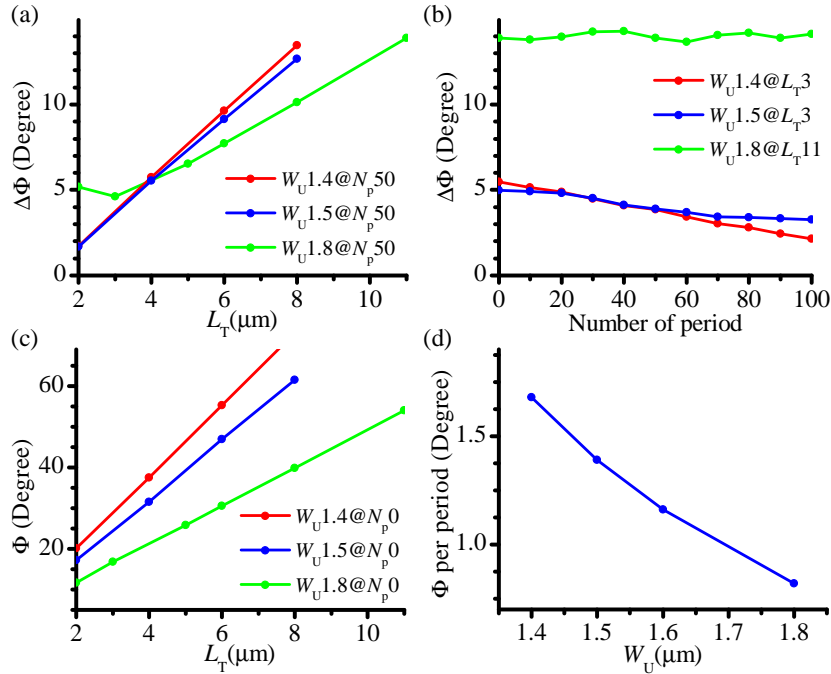


Figure 4. (a)  $\Delta\Phi$  as a function of  $L_T$  for the architectures with different  $W_U$ . (b)  $\Delta\Phi$  as a function of the number of periods for the architectural with different  $W_U$  and  $L_T$ . (c) The phase difference caused by the taper regions as a function of  $L_T$ . (d) The phase difference per period as a function of  $W_U$ .

$L_T = 3 \mu\text{m}$  shows a large variation in the insertion loss, depending on the length of the waveguide. Moreover, its phase shift has a variation  $\Delta\Phi$  of  $\sim 3^\circ$  when the wavelength changes from  $1.45 \mu\text{m}$  to  $1.65 \mu\text{m}$ . Here,  $\Delta\Phi$  is given by  $\Delta\Phi = \max[\Phi(\lambda)] - \min[\Phi(\lambda)]$ .

In some cases, a completely wavelength-independent PS (*i.e.*,  $\Delta\Phi = 0$ ) or a PS with other  $\Delta\Phi$  must be designed. To develop such PSs, we will study the influences of  $W_U$ ,  $W_L$ ,  $L_T$ , and  $N_p$  on  $\Phi$  and  $\Delta\Phi$ . In the following simulations, we use  $W_U - W_L = 200 \text{ nm}$  and a wavelength range of  $1.45 \mu\text{m}$  to  $1.65 \mu\text{m}$ .

When  $N_p = 50$ ,  $\Delta\Phi$  varies with  $L_T$  for  $W_U = 1.8 \mu\text{m}$ ,  $1.5 \mu\text{m}$ , and  $1.4 \mu\text{m}$ , respectively, as shown in Fig. 4(a). We can observe that  $\Delta\Phi$  is linear with  $L_T$  when there is slight multimode interference. As shown in Fig. 4(b),  $\Delta\Phi$  also shows a variation with the number of periods except when  $W_U = 1.8 \mu\text{m}$ . Fig. 4(c) depicts the variation of the phase difference caused by taper regions with  $L_T$  for  $W_U = 1.8 \mu\text{m}$ ,  $1.5 \mu\text{m}$ , and  $1.4 \mu\text{m}$ , respectively. The relationship between phase shift per period and  $W_U$  is shown in Fig. 4(d). Figure 4 provides information useful for designing an arbitrary PS.

### 2.3 Dual Asymmetric SWG PS

From Fig. 4(b), we know that when  $W_U = 1.8 \mu\text{m}$ ,  $\Delta\Phi$  is insensitive to the number of periods. Based on this property, we propose a dual asymmetric SWG PSs that consists of two asymmetric SWG PS as shown in Fig.

5(a). The second asymmetric SWG PS is used to compensate for  $\Delta\Phi$  of the first asymmetric SWG PS so that we set its  $N_p$  at zero. Through compensating in this way, a completely wavelength-independent PS can be achieved. Figure 1(b) indicates that we can obtain any phase shift by changing the  $N_p$ . In this section, we provide an example of how to design a completely wavelength-independent PS using SWG waveguides. We additionally note that arbitrary PSs can also be built using these SWG waveguides. In the following section, we demonstrate how to design a broadband polarimeter with two different PSs.

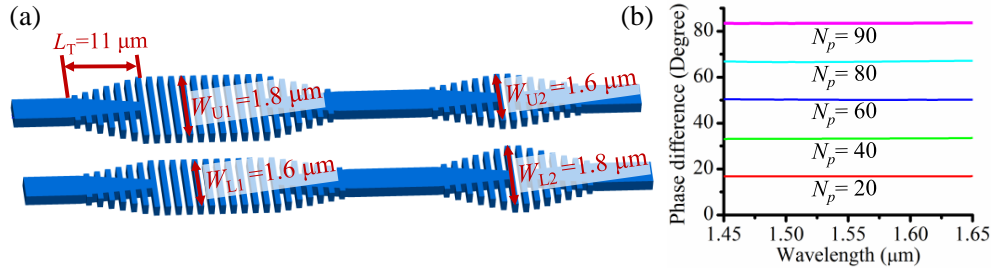


Figure 5. (a) A schematic of the proposed dual asymmetric SWG PS. (b) The phase difference between two paths as a function of the wavelength for different  $N_p$ .

### 3. DESIGN OF POLARIMETER USING SWG WAVEGUIDE

A schematic of the proposed polarimeter is depicted in Fig. 6. A surface polarization splitter is used to couple the incoming light from free space into a PIC chip. Simultaneously, two orthogonal linear polarization states of incoming light are split into two waveguides, respectively. Then, in the PICs, the light sequentially passes through an asymmetric power splitter and crossed coherent analyzer. For the asymmetric power splitter, the output power ratio of the weaker paths and the relatively stronger paths are denoted by  $PR$  and  $(1 - PR)$ , respectively. We set the corresponding phase shift in two paths as  $\varphi_w$  and  $\varphi_s$ , respectively. The crossed coherent analyzer consists of four SWG waveguides. The phase shifts of the four SWG waveguides are represented as  $\theta_1$ ,  $\theta_2$ ,  $\theta_3$ , and  $\theta_4$ , respectively.

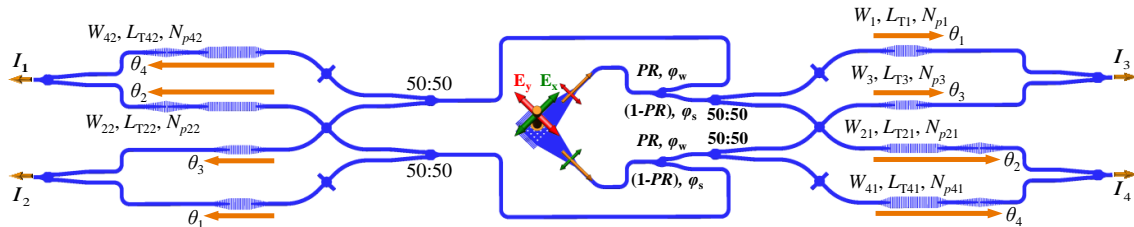


Figure 6. The schematic of the proposed silicon photonic polarimeter.

According to our previous work,<sup>2</sup> when  $(\theta_1 - \theta_3) - (\varphi_w - \varphi_s) = 2n\pi \pm \pi/4$  and  $(\theta_4 - \theta_2) + (\varphi_w - \varphi_s) = 2n\pi \pm 3\pi/4$ , or  $(\theta_1 - \theta_3) - (\varphi_w - \varphi_s) = 2n\pi \pm 3\pi/4$  and  $(\theta_4 - \theta_2) + (\varphi_w - \varphi_s) = 2n\pi \pm \pi/4$  (where  $n$  is an integer), we can obtain an optimal polarimeter in the presence of Gaussian and Poisson shot noise. Here, we select the parameters of  $(\theta_1 - \theta_3) - (\varphi_w - \varphi_s) = \pi/4$  and  $(\theta_4 - \theta_2) + (\varphi_w - \varphi_s) = 3\pi/4$  as an example to design a broadband optimal polarimeter. The optimal polarimeter also requires  $PR/(1 - PR) = 2 - \sqrt{3} \approx 0.2679$ .

Figure 7(a) shows the  $PR/(1 - PR)$  and  $(\varphi_w - \varphi_s)$  of the asymmetric power splitter as a function of wavelength. The variation of the  $PR/(1 - PR)$  is less than 0.05 over a wavelength range of 1.45  $\mu\text{m}$  to 1.65  $\mu\text{m}$ . The mean and variation of the  $(\varphi_w - \varphi_s)$  are 12.81° and 8.28°, respectively. More information about the asymmetric power splitter can be found in our previous work.<sup>7</sup> To compensate for  $(\varphi_w - \varphi_s)$ , the mean and variation of  $(\theta_1 - \theta_3)$  should be 57.81° and 8.28°, respectively. An asymmetric SWG PS with  $W_1 = 1.5 \mu\text{m}$ ,  $W_3 = 1.3 \mu\text{m}$ ,  $L_{T1} = L_{T3} = 5.4 \mu\text{m}$ , and  $N_{p1} = N_{p3} = 11$  was selected to realize such a phase shift. As shown in Fig. 7(b), the variation of  $(\theta_1 - \theta_3) - (\varphi_w - \varphi_s)$  decreases to 4° after compensation. Similarly, the mean and variation of  $(\theta_4 - \theta_2)$  should be 122.19° and  $-8.28^\circ$ , respectively. To achieve a variation of  $-8.28^\circ$ ,

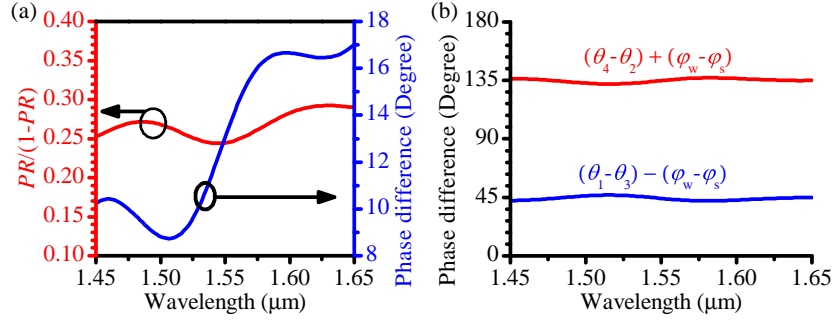


Figure 7. (a)  $PR/(1-PR)$  (red line), and phase difference between two output paths (blue line) of the proposed asymmetric power splitter vary with the wavelength. (b) After compensating,  $(\theta_1 - \theta_3) - (\varphi_w - \varphi_s)$  and  $(\theta_4 - \theta_2) + (\varphi_w - \varphi_s)$  of the proposed polarimeter vary with wavelength.

we cascaded two SWG PSs together as shown in Fig. 6. The structural parameters of the two SWG PSs were:  $W_{21} = 1.3 \mu\text{m}$ ,  $W_{41} = 1.5 \mu\text{m}$ ,  $L_{T21} = L_{T41} = 3 \mu\text{m}$ ,  $N_{p21} = N_{p41} = 108$ , and  $W_{22} = 1.5 \mu\text{m}$ ,  $W_{42} = 1.3 \mu\text{m}$ ,  $L_{T22} = L_{T42} = 6.8 \mu\text{m}$ ,  $N_{p22} = N_{p42} = 0$ . The  $(\theta_4 - \theta_2) + (\varphi_w - \varphi_s)$  as a function of the wavelength is presented in Fig. 7(b).

#### 4. THE PERFORMANCE OF THE PROPOSED POLARIMETER

The incoming Stokes vector  $\mathbf{S}$  can be related to the measured optical intensities by an analysis matrix  $\mathbb{W}$  that

$$\mathbf{I} = \mathbb{W} \cdot \mathbf{S}, \quad (1)$$

where  $\mathbf{S} = (S_0, S_1, S_2, S_3)^T$  is the input Stokes vector, and  $\mathbf{I} = (I_1, I_2, \dots, I_N)^T$  is an  $N$ -dimensional vector representing the measured intensities. The influence of noise on the measured accuracy of the polarimeter can be described by two parameters: condition number  $\kappa$  and equalization factor  $\Delta\gamma$ .<sup>2</sup>

The condition number  $\kappa$  is given by,

$$\kappa = \|\mathbb{W}\| \cdot \|\mathbb{W}^\dagger\|, \quad (2)$$

where  $\mathbb{W}^\dagger$  is the pseudoinverse matrix of  $\mathbb{W}$  and  $\|\cdot\|$  is the matrix norm. Here, we will select Frobenius norms to calculate the condition number.<sup>8</sup> The influence of noise on the measurement accuracy will be at its minimum level when the condition number is minimized. The minimum condition number is equal to  $\sqrt{20}$  when using Frobenius norms. The minimum condition number will be  $\sqrt{3}$  if it is calculated by  $L_2$  norms. As shown in Fig. 8(a), the condition number (blue line) of the proposed polarimeter keeps close to  $\sqrt{20}$  over a wavelength range of 1.45  $\mu\text{m}$  to 1.65  $\mu\text{m}$ . In contrast, the condition number of the polarimeter using traditional waveguide PSs is close to  $\sqrt{20}$  only near 1.55  $\mu\text{m}$ .

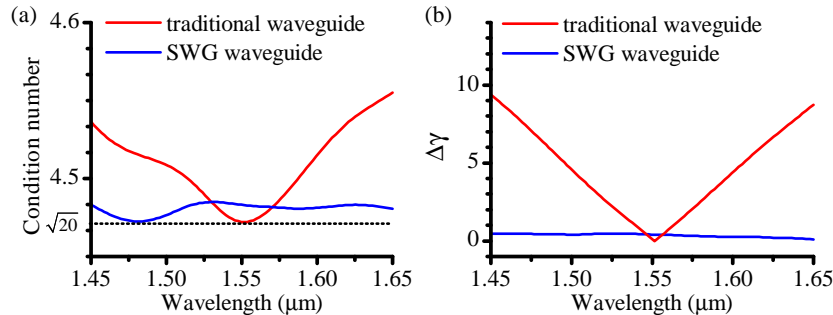


Figure 8. (a) the condition number and (b)  $\Delta\gamma$  of the proposed (blue line) and traditional (red line) devices over a wavelength range of 1.45  $\mu\text{m}$  to 1.65  $\mu\text{m}$ . The minimum condition number is equal to  $\sqrt{20}$  when using Frobenius norms. The minimum condition number will be  $\sqrt{3}$  if it is calculated by  $L_2$  norms.

In the presence of Poisson shot noise, the variance of each Stokes parameter is sensitive to the incoming polarization state except for when the equalization factor  $\Delta\gamma$  is equal to zero.<sup>2</sup>  $\Delta\gamma$  can be obtained by,

$$\Delta\gamma = \frac{1}{3} \cdot \sum_{i=1}^3 (\gamma_i^{max} - \gamma_i^{min}) = \frac{2}{3} \sum_{i=1}^3 \|\mathbf{u}^i\|, \quad (3)$$

where  $\mathbf{u}^i = (Q_{i1}, Q_{i2}, Q_{i3})^T$ , and

$$Q_{ij} = \sum_{n=1}^4 [\mathbf{W}_{(i+1)n}^\dagger]^2 \mathbf{W}_{n(j+1)}. \quad (4)$$

As shown in Fig. 8(b), compared with the polarimeter using the traditional waveguide PSs,  $\Delta\gamma$  of the proposed polarimeter is insensitive to the wavelength and remains close to zero from 1.45  $\mu\text{m}$  to 1.65  $\mu\text{m}$ .

## 5. CONCLUSION

We have theoretically demonstrated the efficacy of a broadband silicon photonic polarimeter based on SWG waveguides. The measurement frame of our proposed device can remain optimal over a wavelength range of 200 nm. The optical properties of the SWG waveguide and the asymmetric SWG PS have been systematically studied, including insertion loss, phase shift caused by taper region, wavelength-dependence of the phase shift, and phase shift per period. Based on these properties, two different PSs were designed to form the proposed device. The broadband device can be integrated with four chip-level spectrometers to create an optimal spectropolarimeter.<sup>9,10</sup> Moreover, this also can work together with the polarization emitter to achieve a chip-scale polarization lidar.<sup>4,11</sup>

## REFERENCES

- [1] Foreman, M. R., Favaro, A., and Aiello, A., "Optimal frames for polarization state reconstruction," *Physical review letters* **115**(26), 263901 (2015).
- [2] Lin, Z., Rusch, L. A., Chen, Y., and Shi, W., "Optimal ultra-miniature polarimeters in silicon photonic integrated circuits," *APL Photonics* **4**(10), 100806 (2019).
- [3] Lin, Z., Rusch, L., Chen, Y., and Shi, W., "Chip-scale, full-stokes polarimeter," *Optics Express* **27**(4), 4867–4877 (2019).
- [4] Lin, Z., Chen, Y., Rusch, L., and Shi, W., "On-chip circular polarization splitter using silicon photonic nanoantenna array," *ACS Photonics* **5**(11), 4338–4342 (2018).
- [5] Uematsu, T., Ishizaka, Y., Kawaguchi, Y., Saitoh, K., and Koshiba, M., "Design of a compact two-mode multi/demultiplexer consisting of multimode interference waveguides and a wavelength-insensitive phase shifter for mode-division multiplexing transmission," *Journal of Lightwave Technology* **30**(15), 2421–2426 (2012).
- [6] González-Andrade, D., Luque-González, J. M., Wangüemert-Pérez, J. G., Ortega-Moñux, A., Cheben, P., Molina-Fernández, Í., and Velasco, A. V., "Ultra-broadband nanophotonic phase shifter based on subwavelength metamaterial waveguides," *arXiv preprint arXiv:1907.07947* (2019).
- [7] Lin, Z. and Shi, W., "Broadband, low-loss silicon photonic y-junction with an arbitrary power splitting ratio," *Optics express* **27**(10), 14338–14343 (2019).
- [8] Foreman, M. R. and Goudail, F., "On the equivalence of optimization metrics in stokes polarimetry," *Optical Engineering* **58**(8), 082410 (2019).
- [9] Lin, Z., Dadalyan, T., Villers, S. B.-d., Galstian, T., and Shi, W., "Chip-scale full-stokes spectropolarimeter in silicon photonic circuits," *arXiv preprint arXiv:2002.02062* (2020).
- [10] Lin, Z. and Lin, J., "Optical nanoantennas as on-chip spectrometer: Discriminating the wavelength of infrared light," *EPL (Europhysics Letters)* **111**(3), 34005 (2015).
- [11] Lin, Z. and Shi, W., "Ultra-compact polarization emitter using a silicon nanoantenna," in [2019 Conference on Lasers and Electro-Optics (CLEO)], 1–2, IEEE (2019).